Nanoscale

PAPER

View Article Online
View Journal | View Issue

Cite this: *Nanoscale*, 2023, **15**, 3893

Assemblies of poly(*N*-vinyl-2-pyrrolidone)-based double hydrophilic block copolymers triggered by lanthanide ions: characterization and evaluation of their properties as MRI contrast agents†

Marjorie Yon,[a] Laure Gibot,[a] Stéphane Gineste,[a] Pascale Laborie,[b] Christian Bijani,[c] Christophe Mingotaud,[a] Olivier Coutelier,[a] Franck Desmoulin,[d,e] Carine Pestourie,[e] Mathias Destarac,[a] Diana Ciuculescu-Pradines *[a] and Jean-Daniel Marty *[a]

Received 23rd September 2022,
Accepted 24th January 2023

DOI: 10.1039/d2nr04691a

rsc.li/nanoscale

Because of the formation of specific antibodies to poly(ethylene glycol) (PEG) leading to life-threatening side effects, there is an increasing need to develop alternatives to treatments and diagnostic methods based on PEGylated copolymers. Block copolymers comprising a poly(*N*-vinyl-2-pyrrolidone) (PVP) segment can be used for the design of such vectors without any PEG block. As an example, a poly(acrylic acid)-*block*-poly(*N*-vinyl-2-pyrrolidone) (PAA-*b*-PVP) copolymer with controlled composition and molar mass is synthesized by reversible addition–fragmentation chain transfer (RAFT) polymerization. Mixing this copolymer with lanthanide cations (Gd^{3+}, Eu^{3+}, Y^{3+}) leads to the formation of hybrid polyion complexes with increased stability, preventing the lanthanide cytotoxicity and *in vitro* cell penetration. These new nanocarriers exhibit enhanced T_1 MRI contrast, when intravenously administered into mice. No leaching of gadolinium ions is detected from such hybrid complexes.

Introduction

Lanthanide based nanomaterials are a very important class of imaging probes in the biomedical field.[1,2] These include, for example, the most successful contrast agents for magnetic resonance imaging (MRI), which benefit from the excellent paramagnetic properties of gadolinium ions, or fluorescent labels which use the luminescent properties of Europium. However, beyond the attractive properties of lanthanide ions, the ligands which escort them play a key role in controlling the performances of the contrast agent: (i) regarding the relationship with the captive lanthanide ion, ligands should be capable of strong and multiple interactions allowing one to reach suitable and efficient concentrations for an optimized signal, to prevent them from leaching and to tune the parameters which influence the desired properties; (ii) regarding the ligand/biological interface, ligands should act as a shield, keeping the toxic lanthanide ions out of contact with the biological media and ensure biocompatibility and transport of the payload with long blood-circulation time and possibly specific recognition.

Double hydrophilic block copolymers (DHBCs)[3–6] have unique advantages for the design of vectors incorporating lanthanide ions.[7–9] Typically, one of the blocks which is ionizable can interact with polyvalent metal ions, spontaneously inducing self-assembly of the copolymer into micelle structures and encapsulation of metal ions into the core, through multiple electrostatic interactions, while the second non-ionizable block forms the shell of micelles in contact with the exterior medium. The negatively ionizable groups of poly (acrylic acid) (PAA), in combination with the obvious advantages of poly(ethylene glycol) (PEG) such as hydrophilicity, biocompatibility, Food and Drug Administration (FDA) approval, stealth behaviour *etc.* make PAA-*b*-PEG block copolymers of choice for loading polyvalent metallic ions.[7–15] These copolymers can be synthesized by reversible deactivation radical polymerization (RDRP) from functional PEG.[16] This requires first the modification of one of the end groups of PEG in one or two synthetic steps.[17,18] These modified PEGs then serve

[a]*Laboratoire des IMRCP, Université de Toulouse, CNRS UMR 5623, Université Toulouse III – Paul Sabatier, France. E-mail: eliza.ciuculescu-pradines@univ-tlse3.fr, jean-daniel.marty@univ-tlse3.fr*
[b]*Plateforme scientifique et technique Institut de Chimie de Toulouse ICT – UAR 2599, Université de Toulouse, CNRS, Toulouse, France*
[c]*LCC-CNRS, Université de Toulouse, CNRS, UPS, Toulouse, France*
[d]*Toulouse NeuroImaging Center (ToNIC), Inserm, University of Toulouse—Paul Sabatier, Toulouse, France*
[e]*CREFRE-Anexplo, Université de Toulouse, Inserm, UT3, ENVT, Toulouse, France*
† Electronic supplementary information (ESI) available: Complementary results. See DOI: https://doi.org/10.1039/d2nr04691a

either as macro-chain transfer agents for the copolymerization of acrylic acid (AA) by reversible addition–fragmentation chain transfer (RAFT) polymerization[19] or as macroinitiators for the copolymerization of acrylic esters by atom transfer radical polymerization (ATRP) followed by ester cleavage.[17] Although PEG synthesis requires specific conditions in the laboratory, its highly industrialized polymerization allows the access to medical grade PEGs with a wide variety of molar masses, and their easy implementation into block copolymers. However, the extensive use of PEGs in biomedical field shows that it may have possible drawbacks, thus there is increasing evidence for unexpected immune responses occurring against PEGylated nanocarriers upon repeated administration, an issue becoming more relevant considering the currently running SARS-CoV2 vaccination campaigns.[20–22] Therefore, there is an urgent need to develop alternatives to not run out of treatments or diagnostic methods[20–22] using PEG-based copolymers. Also, colloids based on the association of PEG-based polymers have limitations related to possible aggregation of PEG-coated NPs during lyophilization.[23]

The substitution of the PEG block with another block offers new perspectives for the preparation of original hybrid polyion complexes (HPICs). These DHBCs would provide new opportunities to enrich the knowledge related to their micellization in the presence of polyvalent metallic ions and to the functionalities of the resulting objects in regard to biomedical applications. In this context, the choice of poly(*N*-vinyl-2-pyrrolidone), PVP, seems especially relevant: PVP is a highly water soluble, biocompatible polymer, with an ability to prevent nanoparticles opsonization.[24–26] It has been used as a plasma expander[27] and it is used as carrier of iodine (Inadine, Aerodine, Betadine) for antiseptic usage.[28] As a food additive, PVP is used as a stabilizer and has the E number E1201.[29]

In addition, the polymerization of *N*-vinyl-2-pyrrolidone (VP) can be controlled by RDRP methods.[30,31] Lastly, the use of hydrophilic PVP in colloid formulations has led to colloids with improved stability thanks to the cryoprotective properties of PVP that prevent aggregation during lyophilization.[32] In association with PAA homopolymer, PVP has been mainly used in the composition of interpolymer complexes, based on cooperative hydrogen bonds.[33–36]

Surprisingly, there are only few examples describing the synthesis of PAA-*b*-PVP diblock copolymers: one by consecutive Cu-mediated ATRP of VP and *t*-butyl acrylate followed by *t*-butyl ester cleavage,[37] and one by direct aqueous RAFT polymerization of AA and VP.[38] Moreover, to our knowledge, only one example has reported the use of PAA-*b*-PVP block copolymer for encapsulation of zinc phthalocyanine and doxorubicine into supramolecular assemblies to achieve chemo-photodynamic therapy but no attempt to assemble them in the presence of polyvalent metallic ions has been reported so far.[37]

We report here a more effective and metal free RAFT synthetic strategy to gain access to a PAA-*b*-PVP block copolymer with controlled composition and molar mass. The formation of HPICs through the interaction of this copolymer with different cations (Gd^{3+}, Eu^{3+}, Y^{3+}) was then studied by scattering techniques, NMR and ATR-FTIR spectroscopy and fluorescence experiments (Scheme 1). The stability of these HPICs in culture medium was addressed, together with their toxicity and interactions with cells, *in vitro*. Finally, their MRI relaxivity in comparison to the one of HPICs based on PAA-*b*-PEG copolymer, was evaluated both *in vitro* and *in vivo* in mice model.

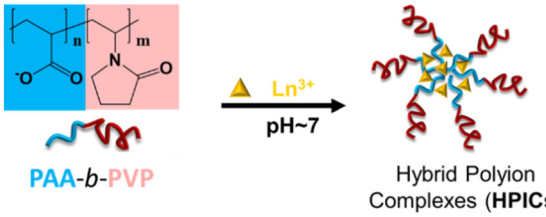

Scheme 1 Strategy of formation of hybrid polyion complexes (HPICs). Lanthanides cations Ln^{3+} were either Gd^{3+}, Eu^{3+} or Y^{3+}.

Results and discussion

Synthesis of PAA-*b*-PVP block copolymer

The synthesis of a PAA-*b*-PVP block copolymer with number-average molar masses (M_n) of respective blocks similar to the ones of PAA_{3k}-*b*-PEG_{6k} which was previously used for the formation of Gd^{3+}-HPICs, was targeted.[7] We did not opt for the direct synthesis of PAA-*b*-PVP by xanthate-mediated aqueous RAFT polymerization[38] as previously reported due to encountered side reactions (acidity-induced formation of *N*-(α-hydroxyethyl)pyrrolidone from NVP) for the M_n and composition of interest. Instead, a PAA-*b*-PVP diblock copolymer was obtained through consecutive RAFT polymerization of methyl acrylate (MA) and VP mediated by *O*-ethyl-*S*-(1-methoxycarbonyl) ethyldithiocarbonate (xanthate XA_1) followed by cleavage of the methyl ester of MA units under basic conditions (Fig. 1A). Unlike direct aqueous synthesis of PAA-*b*-PVP for which average molar masses could not be determined by SEC, this indirect approach allows us to determine the Mn and dispersity of first block and diblock before deprotection by organic SEC: this represents a signification advantage. Polymerization of MA was initiated by azobisisobutyronitrile (AIBN) in the presence of XA_1 at 70 °C in dioxane for 6 h until complete monomer conversion as determined by ^{1}H NMR. A PMA with a $M_{n,NMR}$ of 2750 g mol^{-1} in agreement with the theoretical value was determined by ^{1}H NMR (Table 1 and Fig. S1†). Size exclusion chromatography (SEC) analysis of the PMA showed a monomodal molar mass distribution, with $M_{n,SEC}$ = 2530 g mol^{-1} also in good agreement with the expected M_n and corresponding to a number-average degree of polymerization (DP_n) equal to 32. A dispersity ($Đ$) equal to 1.4 was determined, which is in excellent agreement with the chain transfer constant to XA_1 ($2 < C_{tr,XA1} < 3$) for acrylate monomers.[39] Block copolymerization of VP from the PMA_{32}-XA_1 precursor was successfully carried out in dioxane at 35 °C with 2,2′-azobis(4-methoxy-2,4-dimethylvaleronitrile (V-70) as

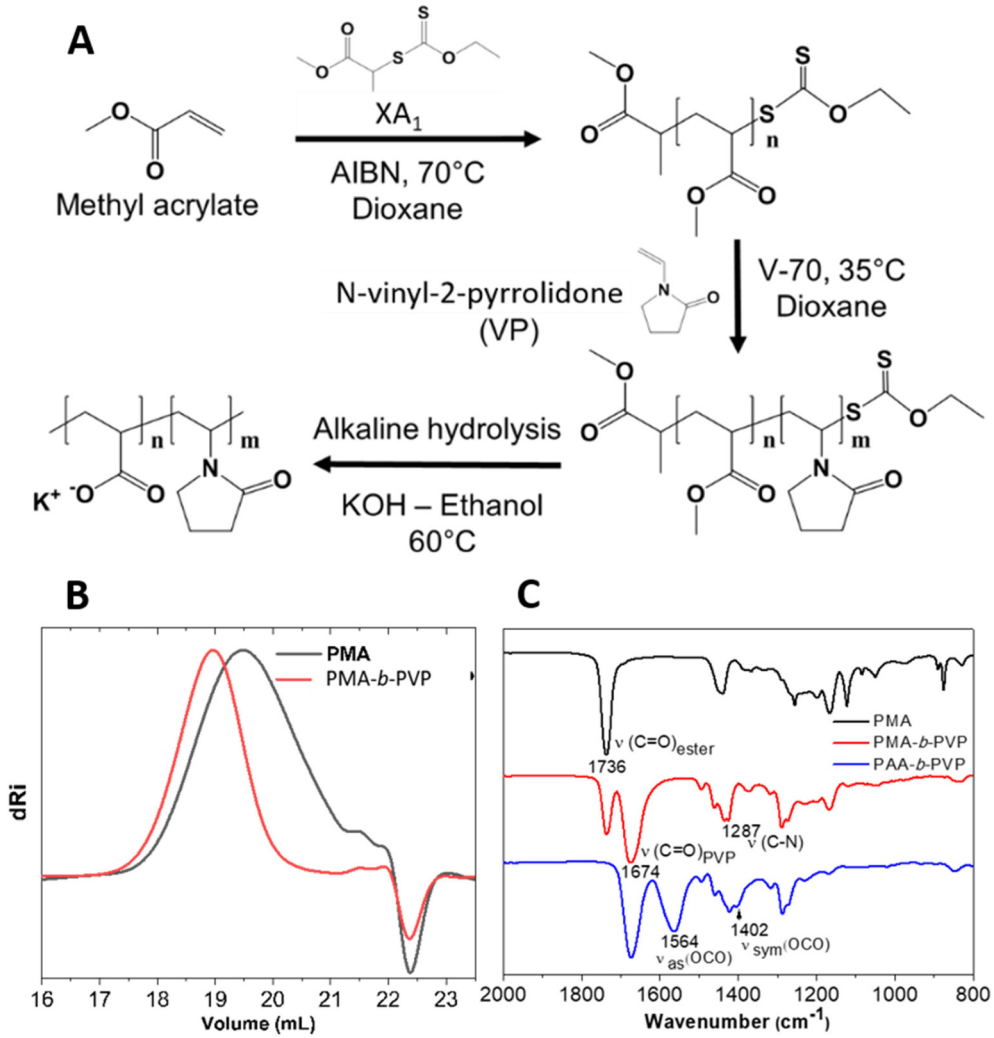

Fig. 1 Synthesis and characterization of PAA-*b*-PVP copolymer. (A) Schematic description of the different steps of the polymer synthesis. (B) Size exclusion chromatograms (RI traces) in DMF/LiBr 10 mM of PMA_{32}-*b*-PVP_{59} (red line) and PMA_{32} (black line). (C) ATR-FTIR spectra of PMA_{32} (black line), PMA_{32}-*b*-PVP_{59} (red line) and PAA_{32}-*b*-PVP_{59} (blue line).

Table 1 SEC and ^{1}H NMR analysis of the synthesized polymers

Polymer	$M_{n,th}$ [a] (g mol^{-1})	$M_{n,NMR}$ [b] (g mol^{-1})	$M_{n,SEC}$ [c] (g mol^{-1}) (*Đ*)	$DP_{n,PVP}/DP_{n,PMA}$ [d] (theoretical value)
PMA	2750	2750	2530 (1.4)	0/32 (0/32)
PMA-*b*-PVP	8300	9400	8630 (1.1)	59/32 (50/30)

[a] $M_{n,th}$ = $[Monomer]_0/[RAFTagent]_0$ × Conversion (Monomer) × MW (Monomer) + MW (RAFT agent). [b] Calculated from ^{1}H NMR (see details in Fig. S1†). [c] Determined by SEC-RI-MALS in DMF/LiBr (10 mM). [d] Calculated from ^{1}H NMR (see Fig. S2,† for details).

evidenced by SEC and ^{1}H NMR analysis (Fig. 1B and Fig. S2†). The molar ratio of PMA to PVP was determined by ^{1}H NMR: PMA/PVP = 0.54 (0.6 expected) leading to a DP_n equal to 59 for the PVP block (see Fig. S2†). Finally, cleavage of ester functions of the PMA block was performed in basic conditions. It could be remarked in the ^{1}H-NMR spectra of the hydrolyzed copolymer (Fig. S3†), the absence of the methyl signal of the ester group at 3.7 ppm. In Fig. 1C, ATR-FTIR spectra also evidenced the disappearance of the carbonyl stretch band of the ester group at 1736 cm^{-1} and the appearance of the carboxylate (OCO) asymmetric and symmetric stretching modes at 1564 cm^{-1} and 1402 cm^{-1}, respectively.

The ^{1}H NMR spectrum of the targeted PAA_{32}-*b*-PVP_{59} block copolymer confirmed its composition (Fig. S3†).

Formation and characterization of HPICs

HPICs were formed by addition of trivalent lanthanide cations (Gd^{3+}, Eu^{3+}, Y^{3+}) to aqueous solutions of the PAA_{32}-*b*-PVP_{59} copolymer followed by the adjustment of the pH to 7. The effect of the addition of increasing amounts of trivalent lanthanide cations was monitored, by dynamic light scattering (DLS) measurements. The ratio, *R*, between the positive charges arising from the trivalent lanthanide cations and the potentially available negative charges from the ionized or ionizable carboxylic acid monomer units of the polymer was

used to define the HPICs: $R = 3{\cdot}[Ln^{3+}]/[AA]$. As an example, mono-angle DLS results for Gd^{3+}/PAA_{32}-*b*-PVP_{59} HPICs solutions are given in Fig. 2A. Similar results obtained for Eu^{3+} and Y^{3+} are given in Fig. S4.† For R values lower than 0.8, the measured light scattering intensity was low. Consequently, the precision and the significance of *Z*-average values obtained from the correlograms are poor and not significant of the presence of colloidal objects. For R larger than 0.8 and up to 1, an increase of scattered intensity was measured associated with a decrease of *Z*-average size. As previously observed in the case of PAA-*b*-PEG copolymer,[8,40] these results suggest the formation of colloids, triggered by the addition of gadolinium ions and achieved for $R = 1$. Around $R = 1$, these colloids exhibit a diameter of *ca.* 25 nm (in term of *Z*-average) with a PDI of 0.27 suggesting a large monomodal distribution or a multimodal distribution. A non-negative least-squares (NNLS) analysis (see Fig. S5†) confirmed the presence of large objects (diameter larger than 100 nm) but at a very small concentration (estimated less than 10^{-2} %). Further multi-angle DLS analysis (Fig. S6†) confirmed that the solution contains mainly Brownian colloids with a radius of 12.1 ± 1.3 nm. Similar sizes were obtained with Y^{3+} and Eu^{3+} ions (respectively 14.3 ± 1.5 nm and 12.2 ± 1.4 nm, Fig. S6†). These values are comparable to the 11.5 ± 1.2 nm radius obtained for HPICs formed by Gd^{3+} and PAA_{3k}-*b*-PEG_{6k} copolymer.[7] Zeta potential was measured as a function of R in order to evaluate the surround-

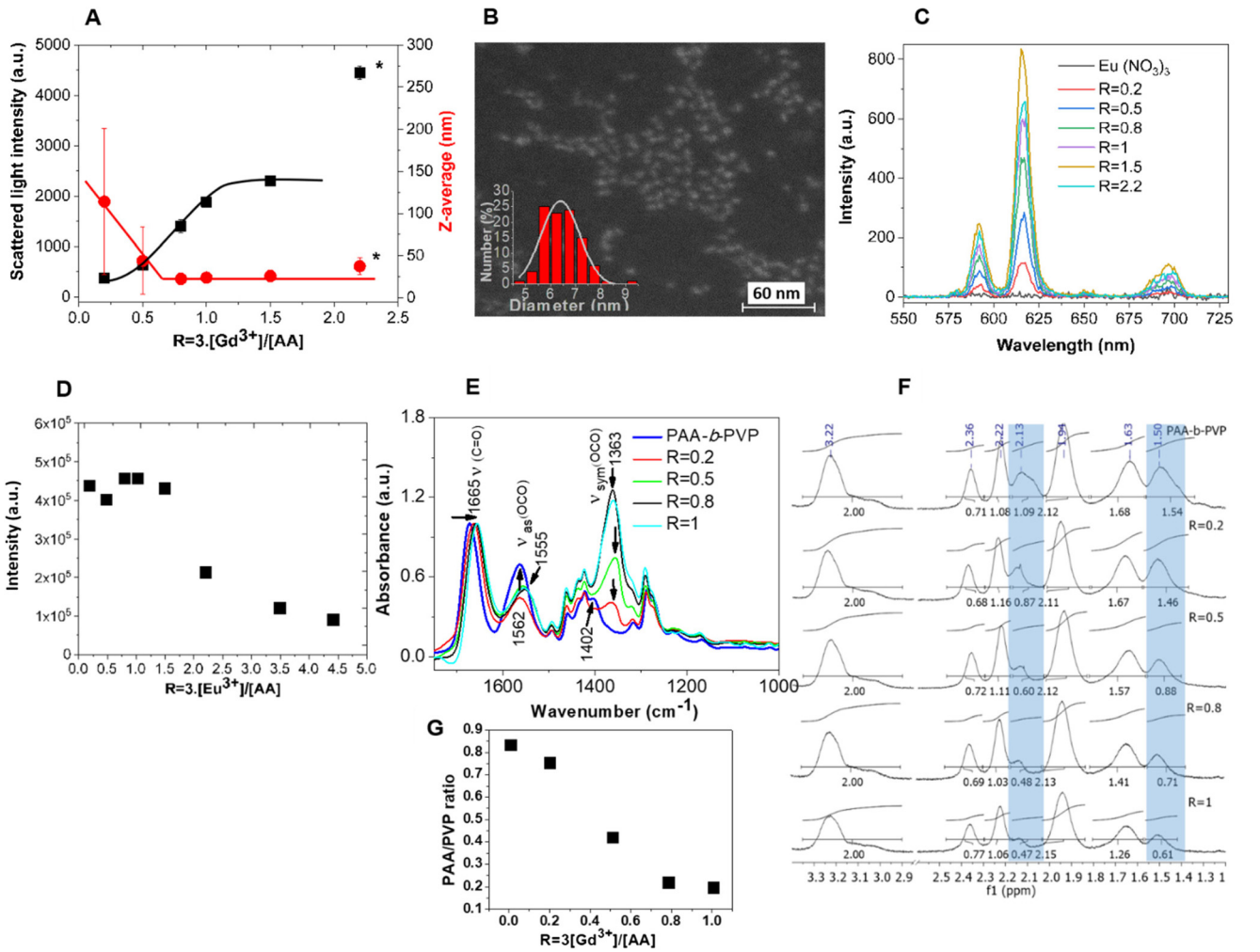

Fig. 2 Characterization of Ln^{3+}/PAA_{32}-*b*-PVP_{59} HPICs. (A) Typical evolutions of the scattered light intensity (black squares) and *Z*-average diameter (red dots), measured by a mono-angle DLS instrument for Gd^{3+}/PAA_{32}-*b*-PVP_{59} HPICs *versus* the R ratio. The lines are just guide for the eyes. Because of self-association of the polymer, the *Z*-average size obtained for R below *ca.* 0.8 corresponds to polydispersed nano-objects. Above R equals to *ca.* 0.8, the size distribution is quasi mono-modal. *At the highest ratio ($R = 2.2$) the formation of hydroxide species were evidenced by ATR-FTIR experiments, so corresponding values do not correspond solely to HPICs formation. (B) Scanning transmission electron microscopy images using high-angle annular dark-field detector (HAADF-STEM) and inset: the respective size distribution histogram. (C) Emission spectra (λ_{ex} = 256 nm) of Eu^{3+}/PAA_{32}-*b*-PVP_{59} HPICs at different R ratios. (D) Normalized intensities of the $^7D_0 \rightarrow {}^7F_2$ transition at 615 nm in respect to the Eu^{3+} concentration as a function of R ratios. (E) ATR-FTIR spectra of PAA_{32}-*b*-PVP_{59} (blue line) and of Gd^{3+}/PAA_{32}-*b*-PVP_{59} HPICs for different R ratios. (F) ^1H NMR spectra of Y^{3+}/PAA_{32}-*b*-PVP_{59} HPICs at different R ratios. (G) Evolution of the integral ratio of the protons associated to the carboxylate block, to the ones of PVP block with the R ratio.

ing electric potential of the colloidal objects (Fig. S7†). Pristine PAA_{32}-*b*-PVP_{59} polymer solutions were found with an overall negative zeta potential value of about $\zeta = -32 \pm 2$ mV at pH 7, which is due to the negatively charged carboxylate groups of the PAA block in solution. Addition of Gd^{3+} ions then induces the decrease of the zeta potential until $R = 1$ where a plateau value at about $\zeta \approx 0$ mV is reached for $R \geq 1$. The objects corresponding to a ratio $R = 1$ were observed by conventional transmission electron microscopy (TEM) (see Fig. S8A†). Even if it was possible to visualize them, the contrast was poor and got worse with the magnification, typical of weakly scattering materials. This is probably due to the relative low density of the gadolinium ions in the polymer matrix sample (very roughly estimated from the PAA density around few gadolinium per nm^3), to the small size of the nanoparticles and to the drying process which could disorganize the HPICs. However, as shown in Fig. S8A,† a mean diameter of the objects of 11.5 nm with a standard deviation $\sigma = 1.5$ nm, obtained by a Gaussian fit could be calculated from such TEM pictures. Additionally, the sample was mapped by scanning transmission electron microscopy using high angle annular dark-field detector (HAADF-STEM) in order to obtain imaging only from incoherently scattered electrons (Rutherford scattering from the nucleus of the atoms) and thus to obtain a better contrast due to variations in atomic number Z of the elements in the sample.[41,42] In Fig. 2B and Fig. S8† the regions containing gadolinium ions appear white in contrast to the polymer. The diameter of the white dots is of 6.4 nm ($\sigma = 0.8$ nm) slightly smaller than the one observed in conventional TEM in agreement with the sequestering of the Gd^{3+} ions in the polymer objects. This estimation of the core size is close to the one measured by ASAXS on other types of HPICs.[15]

Further proofs of the interaction of lanthanides ions with the PAA_{32}-*b*-PVP_{59} copolymer, leading to the formation of well-defined objects, were obtained by investigating the luminescence properties of Eu^{3+} ions and by infrared spectroscopy, respectively. The emission spectra ($\lambda_{ex} = 256$ nm) of Eu^{3+}/PAA_{32}-*b*-PVP_{59} HPICs at different *R* ratios, in aqueous solutions at pH 7 are shown in Fig. 2C.

Strong red emission was detected at 590 nm and 615 nm, corresponding respectively to the $^7D_0 \rightarrow {}^7F_1$ and $^7D_0 \rightarrow {}^7F_2$ transitions of Eu^{3+},[43] while no significant intensity was detected in the emission spectrum of an aqueous solution of $Eu(NO_3)_3$ with a concentration of Eu^{3+} similar to the one in HPICs with $R = 1$. Moreover, the number of water molecules in the first coordination sphere of Eu^{3+} ions, estimated using fluorescence lifetime measurements and the equation proposed by R. M. Supkowski *et al.*[44] was found around 3.7 ± 0.2 water molecules for all *R* ratios. This is significantly lower than the 9 expected for the fully hydrated europium salt in water[45] (see Table S1†). As the emission of Eu^{3+} is highly dependent on its coordinated water molecules, due to non-radiatively deactivation of the $^7D_0$ excited state by energy transfer to the OH vibrational modes of coordinated water molecules,[43] the enhanced emission of Eu^{3+}/PAA_{32}-*b*-PVP_{59} HPICs illustrates that the Eu^{3+} environment is less hydrated in the presence of the copolymer.[46] Coordinated water molecules are replaced by carboxylates units of the copolymer which electrostatically interact with the positively charged Eu^{3+} ions. Additionally up to $R = 1$, Eu^{3+} ions in the HPICs have close coordination environments as shown by the constant values of normalized intensities of the $^7D_0 \rightarrow {}^7F_2$ transition at 615 nm in respect to the Eu^{3+} concentration (see Fig. 2D). For $R > 1$, the decrease of the normalized intensity should correspond to the presence of free (and poorly emitting) europium ions in solution.

The ATR-FTIR spectra of Gd^{3+}/PAA_{32}-*b*-PVP_{59} HPICs, measured as powder solids obtained by lyophilization of the solutions, at different *R* ratios are shown in Fig. 2E. For a better visualization, all spectra were normalized to the absorbance of C=O amide stretching band (at 1665 cm^{-1}) of the pyrrolidone ring of the PAA_{32}-*b*-PVP_{59} polymer. In the polymer at pH 7, the carboxylate (OCO) asymmetric and symmetric stretching modes appeared at 1562 cm^{-1} (ν_{as}) and 1402 cm^{-1} (ν_{sym}), respectively. Addition of Gd^{3+} ions shifted the wavenumbers of the two carboxylate ν_{as} and ν_{sym} bands at 1555 cm^{-1} and 1363 cm^{-1}, respectively. The progressive increase in intensity of these two bands with increasing amount of Gd^{3+} ions until $R = 1$ is especially noteworthy. For higher ratio these intensities remained constant (Fig. S9A†). This behavior is consistent with the progressive neutralization of the negatively charged carboxylate groups of the polymer by the Gd^{3+} ions until $R = 1$. For *R* exceeding the neutralization ratio ($R > 1$), no additional interactions with carboxylate functions were formed. The difference (noted Δ between the wavenumbers of carboxylate symmetric and asymmetric peaks) is frequently used to determine the type of coordination with the metal center.[47,48] For a monodentate bonding, Δ increases compared to the free carboxylate anion; for bidentate chelating coordination Δ decreases and for bidentate bridging, Δ remains similar to the free anion.[47] The higher value of $\Delta = 190$ cm^{-1} in the presence of Gd^{3+} ions and for all *R* ratios, compared to the one of the free carboxylate ($\Delta = 161$ cm^{-1}) suggests a monodentate mode coordination of carboxylates of the polymer to the Gd^{3+} ions. This type of coordination is consistent with the hard acid character of the Gd^{3+} ions, favoring electrostatic interactions with lack of strong directionality in binding donor groups, in the gadolinium first coordination sphere.[49] The complexation between the Gd^{3+} ions and the carboxylate groups of the PAA block until $R = 1$, is also evidenced by the progressive shift to lower wavelength, of the characteristic stretching band of the amide C=O group of the pyrrolidone ring initially at 1665 cm^{-1} up to 1658 cm^{-1}. This complexation releases the NVP units of the PVP block from the self-association with the AA units of the PAA block, and thus the characteristic stretching band of the amide C=O group shifts to lower wavelength, characteristic of a NVP environment in pure PVP, as observed by comparing the ATR-FTIR spectra of the PAA-*b*-PVP copolymer and the PVP homopolymer (Fig. S9C†).

To get more information on the formation of HPICs, ^1H NMR experiments were performed using Y^{3+}. Indeed, yttrium presents coordination chemistry similar to the one of lanthanide ions and it is not paramagnetic.[50] The longitudinal relax-

ation time (T_1) of the protons which can be associated with the mobility of molecular chains was measured (Fig. S10†). The decreasing of the mobility of the PAA chain of the copolymer, due to complexation with the Gd^{3+} ions was evidenced by the increasing of the relaxation time (T_1) of the corresponding protons. The T_1 values were further taken into account to acquire ^{1}H NMR spectra in quantitative conditions and to determine the evolution of the integral ratio of the protons associated to the carboxylate block, to the ones of PVP block. As can be seen on Fig. 2F and Fig. S11 and S12,† while the peaks related to PVP block around 3.22, 2.36, 2.22, 1.94 and 1.63 ppm remained roughly constant, the ones associated to the carboxylate block at 1.5 and 2.1 ppm (respectively due to the hydrogen in β and α of the carboxylate function) progressively disappeared when R increased. Using trioxane as a reference, it was evidenced that both PVP and PAA signals decreased with increasing R ratio (Fig. S12A†). However, the protons relative to PAA block were more impacted than the ones of the PVP block (Fig. S12B†). The selective suppression of these peaks suggests the preferential Y^{3+} binding on PAA residues as expected from the intrinsic chelating capability of acrylates and the rigidification of the PAA block. It confirms the results issued from ATR-FTIR and fluorescence. This might be ascribed to the formation of HPICs with a core–shell structure with a Y^{3+}/PAA core surrounded by a PVP shell. As expected, Eu^{3+} based HPICs presented similar ^{1}H NMR spectra (Fig. S13†).

The amount of free ions as a function of R was assessed by using inductively coupled plasma – mass spectroscopy (ICP-MS) analysis. Free ions were separated from HPICs by an ultra-filtration process. In the case of Gd^{3+} based system, free Gd^{3+} ions were evidenced in solution only for molar ratios R higher than 1. These observations confirm the strong interaction of Gd^{3+} ions with carboxylate functions and are consistent with the former observations on the interaction of Gd^{3+} ions with carboxylate groups in PAA_{3k}-*b*-PEG_{6k} type polymers.[7]

Data from ATR-FTIR, NMR, DLS, TEM and zeta potential supported the formation of HPICs with Gd^{3+}, Eu^{3+}, Y^{3+} ions interacting first with the PAA block. When the R ratio is high enough (approximatively above 0.8), these interactions led to the formation of HPICs nano-objects with a core mainly composed of PAA crosslinked by cations surrounded by a shell mainly composed of PVP as depicted in Scheme 1. The formation of hybrid inorganic/polymeric nanoparticles is complete when the R ratio is close to unity. The polymer architecture appears to be essential as the formation of HPICs could not be observed when a statistical copolymer (from commercial source) was used instead of block copolymer (Fig. S14†). The obtained structure is similar in term of architecture and average size to the one obtained with PAA_{3k}-*b*-PEG_{6k} copolymer.[7] Nevertheless, it has to be noted that some differences appear for higher ratios. Indeed, for ratios larger than 2 and on the contrary to what was observed with PAA_{3k}-*b*-PEG_{6k} copolymers, a slight flocculation was observed and could be related to an undefined mixture of gadolinium hydroxide and polymers. Hence, for ratios $R > 1$, beyond the composition assuring the neutralization of carboxylates by Gd^{3+} ions, the infra-red spectra at pH 7 shown clear evidence of the appearance of gadolinium hydroxides (Fig. S9†). The bands at 745 cm^{-1} and 814 cm^{-1} are characteristic of the bending vibrations of Gd–O–H (δOH and γOH, respectively).[51–56] At 1627 cm^{-1} the O–H stretching vibration appears as a shoulder to the C=O amide band of pyrrolidone ring. Such a phenomenon was not observed for PAA_{3k}-*b*-PEG_{6k} probably due to the poor interaction of PEG moieties with hydroxides species.[7] Interestingly for $R < 1$ and at pH 7 the complexation of ions with carboxylate prevent the formation of such hydroxides. The ratio $R = 1$ was chosen for the following experiments.

Colloidal stability of HPICs in biological medium

The colloidal behavior of HPICs ($R = 1$) was assessed in high ionic strength conditions by addition of NaCl solutions of concentration up to 2 mol L^{-1}. No substantial aggregation was evidenced through DLS measurements up to 1 mol L^{-1} NaCl (Fig. 3A and Fig. S15†). A slight loss of the scattered light intensity is indicative of the presence of some aggregates beyond 1 mol L^{-1} NaCl. This result is in good agreement with quasi null zeta potential value indicating that the colloidal stability of these HPICs objects does not rely on electrostatic stability but rather on steric stabilization supported by hydrated PVP chains on the corona of the HPICs architecture. DLS measurements within 2 weeks demonstrated the stability of the HPICs with time, without any release of Gd^{3+} ions being detected. It is noteworthy the stability of the HPICs down to a pH of 5 as demonstrated by DLS and fluorescence measurements (Fig. S16†), meaning that these objects could be used to image the acidic extracellular environment of tumors. The integrity of HPICs was also maintained with high dilution (up to 50 times) (Fig. 3B and Fig. S17†). Stability over this range of dilution demonstrates that the NPs are not in equilibrium with a large quantity of free copolymers and Gd^{3+} ions.

A key issue concerns the stability of HPICs in complete cell culture medium containing 10% of fetal bovine serum (FBS). Nevertheless, attempts to evidence the presence of HPICs by tracking their light scattering failed because of the presence of fetal bovine serum rich in proteins and lipids with considerable sizes. (Fig. S18A†) However, in serum-free cell culture medium (without proteins but rich in inorganic salts such as: carbonate, phosphate, chloride and nitrate) the integrity of the Eu^{3+}/PAA_{32}-*b*-PVP_{59} HPICs could be evidenced by DLS (Fig. S18A†). In contrast, $Eu(NO_3)_3$ forms big aggregates in this medium[57] (Fig. S18B†). To further investigate the HPICs stability in complete cell culture medium, luminescent measurement were performed by using Eu^{3+} HPICs as a valuable luminescent probe.[1,55,56] In order to remove the parasite fluorescence signals mainly arising from red phenol fluorescence present in complete cell culture medium, time-resolve detection experiments were performed.[58] As shown in Fig. S18C,† the luminescence intensity of $Eu(NO_3)_3$ is significantly increased both in complete cell culture medium and serum free culture medium compared to water, confirming the complexation of Eu^{3+} ions by the constituents present in these

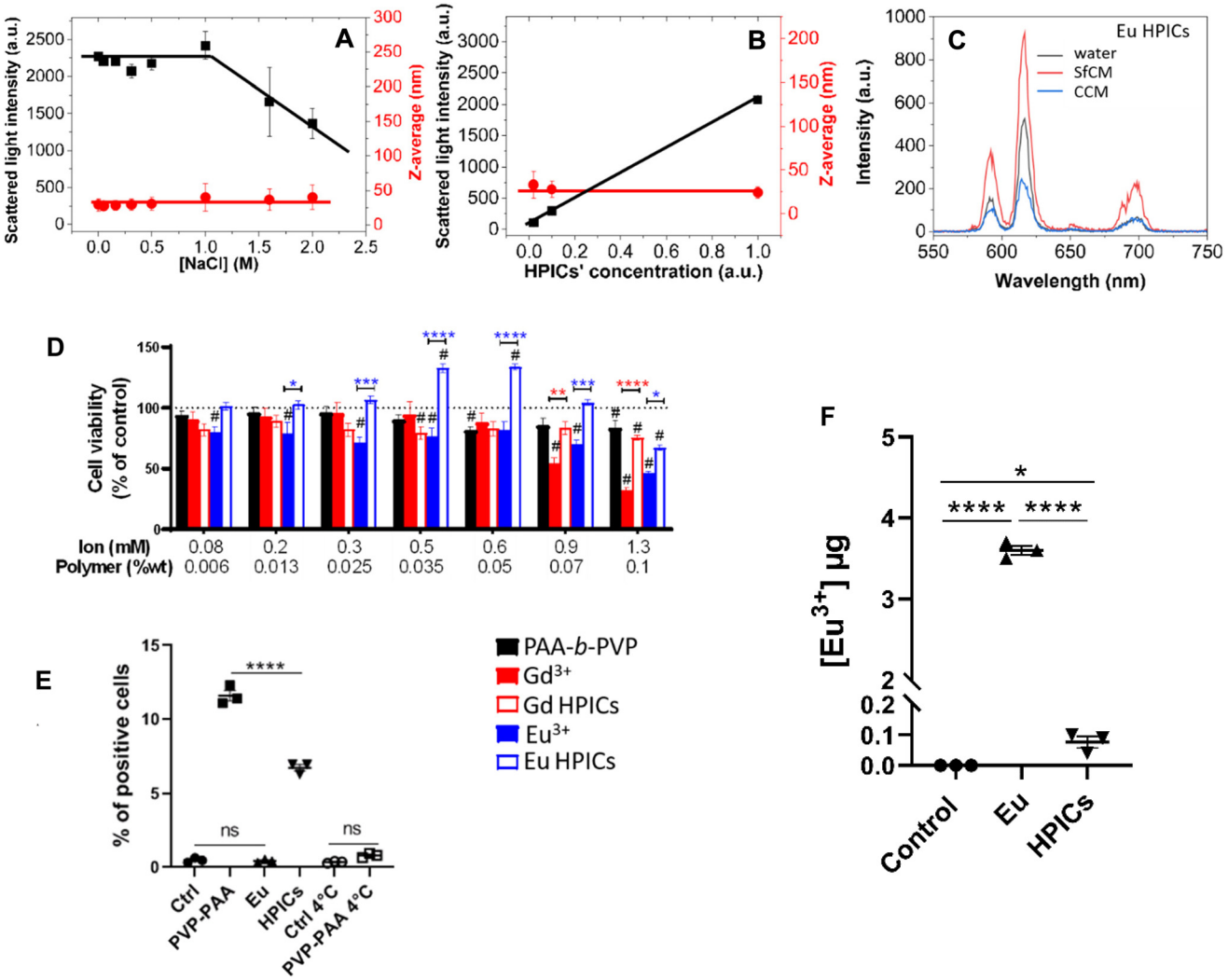

Fig. 3 Assessment of HPICs colloidal stability, cytotoxicity and cell penetration. (A) Colloidal stability of Gd^{3+} HPICs in high ionic strength conditions as determined by mono-angle DLS measurements: the average diameter of the HPICs remains constant with the addition of the increasing concentrations of NaCl. (B) Evidence of the constant diameter of Gd^{3+} HPICs with the dilution as measured by mono-angle DLS. The scattered light intensity decreases due to the dilution. The lines are just guide for the eyes. (C) Time-resolved emission spectra (λ_{ex} = 256 nm) of Eu^{3+} HPICs in different media (SfCM for serum free culture medium and CCM for complete cell culture medium). (D) Quantification of HPICs cytotoxicity on human colorectal tumor cells HCT-116 after 48 h of treatment. n = 6. Data are represented as mean ± SEM. Statistical differences were analyzed either by 1-way ANONA followed by Dunnett's multiple comparisons post-test for each condition compared to the control one "no treatment" (# symbols, $p < 0.05$) or by 2-way ANOVA followed by Turkey's post-test to compare conditions with each other (blue or red stars, *$p < 0.05$; **$p < 0.01$; ***$p < 0.001$; ****$p < 0.0001$). (E) Flow cytometry analysis of PAA_{32}-b-PVP_{59} levels in HCT-116 cells when incubated over 6 h with PAA_{32}-b-PVP_{59} alone, $Eu(NO_3)_3$ and Eu^{3+} HPICs and for condition of incubation at 4 °C. Statistical analysis by 1-way ANOVA followed by Tukey's multiple comparisons test. Ns = non-significant; **** = $p < 0.0001$. Data are represented as a mean value ± SEM. (F) ICP-MS analysis quantifying penetration of free Eu^{3+} and of Eu^{3+} in PAA_{32}-b-PVP_{59} HPICs in HCT-116 cells. Statistical analysis by unpaired-t test. * = $p < 0.05$, **** = $p < 0.0001$. Data are represented as a mean value ± SEM.

media.[57] The luminescence intensity of Eu^{3+}/PAA_{32}-b-PVP_{59} HPICs is also modified in both media (Fig. 3C). The medium-dependent variation in intensity follows the order: serum-free culture medium, water and complete cell culture medium. Moreover, the ratio of the luminescent intensity of the transition bands $^5D_0 \rightarrow {}^7F_2$ (615 nm) to $^5D_0 \rightarrow {}^7F_1$ (590 nm), the first one being solely dependent on the environment, decreases by 22% from 3.2 in water to 2.5 in serum-free culture medium and by 28% in complete cell culture medium.[43,56,59] Despite the nearly identical fine structure of the luminescence spectra of Eu^{3+}/PAA_{32}-b-PVP_{59} HPICs and $Eu(NO_3)_3$ in the different media, they do not match at all, demonstrating a different and specific chemical environment of Eu^{3+} ions in these two samples and the role of the PAA_{32}-b-PVP_{59} polymer in the protection of Eu^{3+} ions. In addition, the luminescence intensity of Eu^{3+}/PAA_{3k}-b-PEG_{6k} HPICs in complete cell culture medium is much more affected than Eu^{3+}/PAA_{32}-b-PVP_{59} HPICs one (see Fig. S18D†). Based on the spectroscopic finding, it could be concluded that the HPICs are affected by the culture medium[57] but that HPICs based on

PAA-*b*-PVP are more stable in such complex environment. However, the exact description of the nature of the interaction of HPICs with the serum protein is not trivial and is the scope of a future work.[60]

HPICs *in vitro* prevent lanthanides cytotoxicity and cell penetration

Cytotoxicity of the different elements forming the PAA_{32}-*b*-PVP_{59} HPICs was assessed *in vitro*, in complete cell culture medium, on human colorectal tumor cells HCT- 116. Cell viability was measured using PrestoBlue assay. For that purpose, cells were incubated for 48 h with increasing concentrations of polymer PAA_{32}-*b*-PVP_{59}, $Eu(NO_3)_3$ or $Gd(NO_3)_3$ aqueous solutions, and Eu^{3+}/PAA_{32}-*b*-PVP_{59} HPICs or Gd^{3+}/PAA_{32}-*b*-PVP_{59} HPICs (Fig. 3D). Results concerning the polymer PAA_{32}-*b*-PVP_{59} show a limited cytotoxicity toward HCT-116, since at the highest concentration (0.1 wt%) at least 80% of cells were viable. This is considerably more than the viability (only 50%) of the HCT-116 cells observed for PAA_{3k}-*b*-PEG_{6k} copolymer at 0.09 wt%.[8] Eu^{3+} ions from $Eu(NO_3)_3$ significantly and statistically affect cell viability, over the whole range of concentrations used. For Gd^{3+} ions from $Gd(NO_3)_3$ cell viability decreases to less than 50% at 0.9 mM. In a remarkable manner, when these ions were encapsulated within the PAA_{32}-*b*-PVP_{59} HPICs structure, their cytotoxcity undoubtedly and statistically decreased. Thus, the HPICs were better tolerated than the free Gd^{3+} or Eu^{3+} ions especially at the highest concentrations. These results point to the beneficial role of the PAA_{32}-*b*-PVP_{59} polymer for decreasing toxicity of the lanthanide ions, even that their environment is affected by the complete cell culture medium as demonstrated above. A similar decrease in cytotoxicity was observed when lanthanide was encapsulated in PAA_{3k}-*b*-PEG_{6k} polymer.[8] The proliferative effect of Eu-HPICs at certain concentrations can be noted, a phenomenon that we are not currently able to explain in terms of the biological mechanisms involved. In order to study the Eu^{3+}/PAA_{32}-*b*-PVP_{59} HPICs cell uptake, flow cytometry experiments were performed. For that purpose, HCT-116 cells were incubated for 6 h with 0.07 wt% PAA_{32}-*b*-PVP_{59}, 0.9 mM $Eu(NO_3)_3$ aqueous solution and the corresponding Eu^{3+}/PAA_{32}-*b*-PVP_{59} HPICs (Fig. 3E). As expected, no fluorescence coming from Eu^{3+} was detected due to technical limitations of the conventional, dedicated to biology cytometer, *i.e.* excitation laser and simultaneous fluorescence detection was clearly not optimal for Eu^{3+} excitation.[61]

However, fluorescence signal (Excitation = 405 nm, Emission Max = 711 nm) was detected for the samples incubated with PAA_{32}-*b*-PVP_{59} polymer, due to autofluorescence of the PVP block of the polymer.[62] This represents a real advantage compared to the non autofluorescent PAA_{3k}-*b*-PEG_{6k} copolymer, thus avoiding the use of additional fluorescent dyes. It was found that the percentage of cell labelling is low. 12% of the cell population was labelled in the presence of PAA_{32}-*b*-PVP_{59} copolymer and twice less, approximately 7% in the presence of Eu^{3+}/PAA_{32}-*b*-PVP_{59} HPICs.

Interestingly, when incubation with copolymer was performed at 4 °C, no fluorescent signal was observed within the cells, meaning that endocytosis is a major actor in the process of internalization of the copolymer. Complementary, for the quantification of europium inductively coupled plasma-mass spectrometry (ICP-MS) was used. The quantity of Eu^{3+} ions, when the cells were incubated with 0.9 mM of $Eu(NO_3)_3$, amounts to about 23.6 nmol $Eu^{3+}/20 \times 10^6$ cells after 6 h of exposure, comparable with the value reported for Eu^{3+} ions uptake into FaDu cells.[57] (Fig. 3F) The amount of Eu^{3+} ions decreases at 0.5 nmol $Eu^{3+}/20 \times 10^6$ cells, when the cells were incubated with Eu^{3+}/PAA_{32}-*b*-PVP_{59} HPICs containing 0.9 mM of Eu^{3+} ions. This is in agreement with the low percentage of labelling found by flow cytometry experiments. Furthermore, these results correlate to the cell viability data. Thus our results underline that HPICs organization prevents lanthanide ions and polymer cytotoxicity and cell penetration compared to their free counterparts, mainly by increasing architecture stability of the nanocarrier.

Gd^{3+} HPICs demonstrate increased r_1 relaxivity and enhanced MRI signal on mice

The relaxivity of both types of Gd^{3+} HPICs, formulated either with PAA_{32}-*b*-PVP_{59} or PAA_{3k}-*b*-PEG_{6k} copolymers, was determined in the absence and presence of complete cell culture medium (Fig. S19†). In water, the r_1 relaxivity of Gd^{3+}/PAA_{32}-*b*-PVP_{59} HPICs was measured to be 42 ± 0.36 mM^{-1} s^{-1} (25 °C, 0.47T) very close to the one measured for Gd^{3+}/PAA_{3k}-*b*-PEG_{6k} HPICs in the same conditions *i.e.* 33 ± 0.36 mM^{-1} s^{-1} (whereas a value equal to 48 ± 2 mM^{-1} s^{-1} was measured at 1.4T).[7] However, when mixed with the complete cell culture medium the r_1 relaxivity falls at 12 ± 1.02 mM^{-1} s^{-1} and 11 ± 0.85 mM^{-1} s^{-1} for Gd^{3+}/PAA_{32}-*b*-PVP_{59} and Gd^{3+}/PAA_{3k}-*b*-PEG_{6k} HPICs, respectively (Table 2). This behavior is consistent with the modifications of the HPICs in complete cell culture medium as suggested by luminescence experiments. But still, the values are larger than the values displayed by commercial molecular complexes which are lower than 6 mM^{-1} s^{-1} in human plasma at 37 °C and 0.47T.[63]

Similar values of r_1 relaxivity were measured on micellar systems based on Gd chelates[64,65] or on compounds based on other paramagnetic ions such as Mn^{2+} or Fe^{3+}.[66,67] However, their fabrication is less straightforward than the system that we propose which in comparison is very simple and avoid the use of specific ligands and additional chemicals.

Table 2 Values of the longitudinal relaxivities (r_1) for the HPICs and $Gd(NO_3)_3$ in water and cell culture medium

	Relaxivity r_1 (mM^{-1} s^{-1})		
Medium	Gd^{3+}/PAA_{32}-*b*-PVP_{59}	Gd^{3+}/PAA_{3k}-*b*-PEG_{6k}	Gd^{3+}
Water	42 ± 0.36	33 ± 0.36	13 ± 0.96
Complete cell culture medium	12 ± 1.02	11 ± 0.85	6.4 ± 0.31

The insignificant cytotoxicity of the Gd^{3+}/PAA_{32}-*b*-PVP_{59} HPICs up to 1.3 mM Gd (0.1 wt% of polymer) allowed one to perform *in vivo* experiments on mice and to obtain preliminary determinations of MR contrast efficacy, pharmacokinetic properties, and tolerance. The *in vivo* MR contrast was assessed after intravenous (IV) bolus injection of Gd^{3+}/PAA_{32}-*b*-PVP_{59}

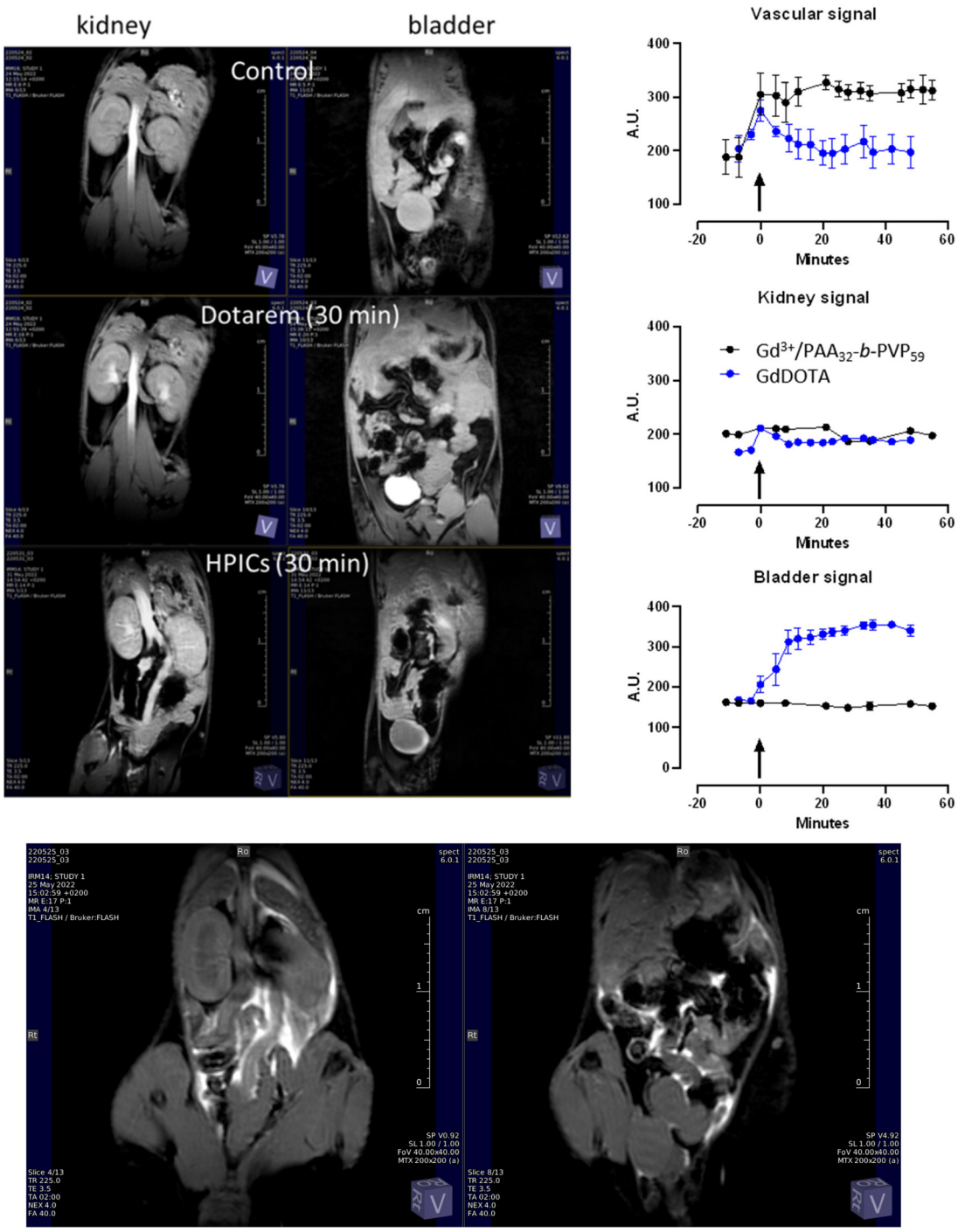

Fig. 4 Assessment of MR contrast efficacy on mice. (A) Coronal T_1-weighted images 30 min after injection of GdDOTA (middle), Gd^{3+}/PAA_{32}-*b*-PVP_{59} HPICs (bottom) in comparison with a control (top). The images were centered on the kidneys (left) and bladder (right). (B) Typical evolution of the MRI signal following the administration (arrow) of GdDOTA (blue) or Gd^{3+}/PAA_{32}-*b*-PVP_{59} HPICs (black) from the vascular space (rectangular shaped ROI taken in the slice at the level of the inferior vena cava, the kidney (ellipse shaped ROI taken in a horizontal image covering all the right kidney) and in the Bladder (circular shaped ROI taken in an horizontal image covering all the Bladder). A.U. (arbitrary unit of the MRI signal expressed as mean value ± SD measured in ROIs). (C). Horizontal slices of the abdomen acquired after 40 min following the intraperitoneal administration of Gd^{3+}/PAA_{32}-*b*-PVP_{59} HPICs. Cut at the kidney level on the left and at the level of the bladder on the right.

HPICs and compared to the use of GdDOTA with an equivalent Gd concentration. Tissue uptake and elimination properties were evaluated using a T_1-weighted dynamic sequence of coronal images centered on the abdominal cavity, acquired during 30 min after IV injection of Gd^{3+}/PAA_{32}-*b*-PVP_{59} HPICs or GdDOTA at 15 μmol kg^{-1} equivalent Gd concentration. In Fig. 4A, regions of interest are given corresponding to the renal cortex of both kidneys and the bladder. Comparatively to GdDOTA, Gd^{3+}/PAA_{32}-*b*-PVP_{59} HPICs significantly increased contrast in all the studied organs: an enhanced contrast of about +67% was measured in T_1-weighted images of the intravascular space for Gd^{3+}/PAA_{32}-*b*-PVP_{59} HPICs after 30 minutes (1% for GdDOTA, Fig. 4A and B) and showed similar trends than the ones previously measured with Gd^{3+}/PAA_{3k}-*b*-PEG_{6k} HPICs.[7] In addition, elimination process for the Gd^{3+}/PAA_{32}-*b*-PVP_{59} HPICs was followed by monitoring signal enhancement *vs.* time in the intravascular space, the kidney and the bladder. (Fig. 4B) Whereas GdDOTA was quickly eliminated from the blood circulation as assessed by the high signal intensity in the bladder after 30 min, Gd^{3+}/PAA_{32}-*b*-PVP_{59} HPICs residence time was relatively long showing a persistent enhancement of the vascular signal. Moreover, direct injection in pelvis enabled to estimate the *in vivo* colloidal stability of Gd^{3+}/PAA_{32}-*b*-PVP_{59} HPICs (Fig. 4C). Indeed, whereas GdDOTA, slowly diffuse out of the peritoneal cavity, contrast enhancement remained confined to the intraperitoneal cavity for the Gd^{3+}/PAA_{32}-*b*-PVP_{59} HPICs indicating the non-penetration of the pelvic barrier of the HPICs and no leak of the Gd^{3+} ions out of the $HPIC_S$. Quantitative biokinetic studies are still needed, but these preliminary studies of a relatively simple HPIC, apparently not toxic to mice, showed surprisingly good stability and superior magnetic relaxivity properties *in vitro* and *in vivo*, even at high magnetic field.

Conclusions

In this work, we demonstrated the pertinence of using a double hydrophilic block copolymer including a PVP block as alternative to the frequently used PEG one, for the elaboration of lanthanide HPICs. For the first time, lanthanide ions were associated to a PAA-*b*-PVP block copolymer. This seldomly reported combination of blocks was successfully achieved through a straightforward methodology based on RAFT polymerization. It was demonstrated that these new HPICs showed similar well-defined architectures, size and size distribution as the analogues based on PAA-*b*-PEG copolymer. The PAA-*b*-PVP copolymer had low toxicity alone and effectively contributed to the decrease of the toxicity of the lanthanide ions when they were embedded into the HPICs. Despite clear evidence of interaction with the serum proteins from the complete cell culture medium, which partially alters the fluorescence and relaxivity properties, the composition of the HPICs seems to be still mostly unaffected which is not the case of the PAA-*b*-PEG analog. This is supported *in vitro* by a low toxicity and low cell penetration of the HPICs compared to their individual constituents and *in vivo* by the impossibility of these HPICs to penetrate the pelvic barrier of mice, with no leak of the Gd^{3+} ions as demonstrating by monitoring the magnetic resonance contrast of the peritoneal cavity.

Finally, the PAA-*b*-PVP HPICs showed enhanced T_1-MRI contrast compared to the GdDOTA (of about +67% measured in T_1-weighted images of the intravascular space after 30 minutes after intravenous injection into mice) and equivalent relaxivity efficiency compared to the PAA-*b*-PEG analogues, thus contributing as a new interesting probe to be used in MRI.

This work paves the way to future studies aiming at developing original HPICs based on new architectures of AA/VP copolymers, supported by the versatility of xanthate-mediated RAFT polymerization.

Experimental methods

Chemicals

(2,2′-Azobis(4-methoxy-2,4-dimethylvaleronitrile) (V-70) (Wako Chemicals), 1,3,5-trioxane (≥99%) (Sigma Aldrich), diethyl ether and absolute ethanol (VWR), *N*,*N*-dimethylformamide anhydrous (99.8%) (Sigma Aldrich), potassium hydroxide (KOH) (Sigma Aldrich), $Gd(NO_3)_3{\cdot}6H_2O$ (99.99% trace metals basis) (Sigma Aldrich), $Eu(NO_3)_3{\cdot}5H_2O$, (99.9% trace metals basis) (Sigma Aldrich), $Y(NO_3)_3{\cdot}6H_2O$ (99.8% trace metals basis) (Sigma Aldrich), NaCl, ACS, (99.0% min.) (Alfa Aesar), were used as received. 1,4-Dioxane (≥99.0%) (VWR) and methyl acrylate (99%, contains ≤100 ppm monomethyl ether hydroquinone as inhibitor) (Sigma Aldrich) were filtrated on alumina. 1-Vinyl-2-pyrrolidone (NVP) (purum, ≥97.0% (GC)) (Sigma Aldrich) was distilled prior to use. 2,2′-Azobis(2-methylpropionitrile) (98%) (AIBN) (Sigma Aldrich) was recrystallized from methanol and dried at room temperature under vacuum. The methyl 2((ethoxycarbonothioyl)thio)-propanoate RAFT agent (XA_1) was synthesized according to a previously published procedure.[68] The statistical PAA_{416}-*r*-PVP_{270} copolymer was purchased from Polymer Source.

Polymer synthesis

Synthesis of PAA_{32}-*b*-PVP_{59} block copolymer. *Step 1: Synthesis of a poly(methyl acrylate)-xanthate macro RAFT agent (PMA-XA_1)*: XA_1 (0.77 g, 3.7×10^{-3} mol), methyl acrylate MA (10 g, 12×10^{-2} mol), 1,4-dioxane (5 g, 5.7×10^{-2} mol), AIBN (61 mg, 3.7×10^{-4} mol) and 1,3,5-trioxane (0.1 g, 1.1×10^{-3} mol) were introduced at room temperature in a Schlenk flask. The reaction mixture was degassed by purging with argon for 30 min, heated and stirred at 70 °C for 6 hours. The polymerization mixture was then cooled down at room temperature, a sample withdrawn and analyzed by ^{1}H NMR to access the monomer conversion (98%) and the solvent was evaporated using a rotary vacuum evaporator. The obtained polymer was characterized without further purification by ^{1}H NMR (Fig. S1†) (300 MHz in $CDCl_3$) δ ppm: 1.3–1.6 (2H, –C**H**$_2$–CH(CO_2CH_3)–S(C═S)–OEt), 1.3–1.6 (3H, C**H**$_3$–CH_2–O– end-group),

1.6–1.8 (2(n − 1)H, –C**H**$_2$–CH(CO_2CH_3)–), 2.25–2.5 (1(n − 1)H, –CH_2–C**H**(CO_2CH_3)–, 3.7 (3(n + 1)H, –CO_2C**H**$_3$), 4.4 (1H, –CH_2–C**H**(CO_2CH_3)–S(C═S)–OEt), 4.7 (2H, CH_3–C**H**$_2$–O– end-group). The degree of polymerization (DP_n) was calculated by as presented in Fig. S1.† $M_{n,th}$ = 2750 g mol^{-1}. $M_{n,NMR}$ = 2750 g mol^{-1}; ATR-FTIR spectroscopy: ν(C═O) ester group = 1736 cm^{-1}.

Step 2: Block copolymerization of 1-vinyl-2-pyrrolidone (NVP) in 1,4-dioxane. The macro-RAFT agent (PMA-XA_1) from step 1 (2 g, 7 × 10^{-3} mol), NVP (3.8 g, 3.4 × 10^{-2} mol), 1,4-dioxane (3.5 g, 4 × 10^{-2} mol), V-70 (46 mg, 1.5 × 10^{-4} mol) and 1,3,5-trioxane (0.1 g, 1.1 × 10^{-3} mol) were introduced at room temperature in a Schlenk flask. The reaction mixture was degassed by purging with argon for 30 min, heated and stirred at 35 °C for 12 hours. The reaction mixture was then cooled down at room temperature and a sample was withdrawn to measure NVP conversion (97%) and calculate the DP_n of the PVP block by ^{1}H NMR analysis (Fig. S2†): (300 MHz in $CDCl_3$) δ ppm: 1.20 (3H, C**H**$_3$–CH_2–O– end-group), 1.30–1.5 (2mH, –N–CH_2–C**H**$_2$–CH_2–CO(N)), 1.6–1.8 (2nH, –C**H**$_2$–CH(CO_2CH_3)–), 2.0–2.18 (2mH, –C**H**$_2$–CH($NCH_2CH_2CH_2CO$(N))–), 2.18–2.25 (1nH, –CH_2–C**H**(CO_2CH_3)), 2.25–2.5 (2mH, –N–CH_2–CH_2–C**H**$_2$–CO(N)), 3–3.5 (2mH, –N–C**H**$_2$–CH_2–CH_2–CO(N)), 3.7 (3(n + 1)H, –CO_2C**H**$_3$), 3.8–4.0 (1mH, –CH_2–C**H**($NCH_2CH_2CH_2CO$(N))–), 4.6 (2H, CH_3–C**H**$_2$–O– end-group) ($M_{n,th}$ = 8300 g mol^{-1}. $M_{n,NMR}$ = 9300 g mol^{-1}. The final composition was established as PMA_{32}-*b*-PVP_{59}. ATR-FTIR spectroscopy: ν(C═O) ester group = 1736 cm^{-1} and ν(C═O) PVP ring = 1674 cm^{-1}. For the purification, the crude reaction solution was precipitated in diethyl ether, filtrated and dried in a vacuum oven over night to remove solvent traces.

Step 3: Hydrolysis of PMA-b-PVP to form PAA-b-PVP. The PMA-*b*-PVP copolymer obtained in step 2 (4.5 g, 5.4 × 10^{-4} mol), ethanol (15.8 g, 0.34 mol) and potassium hydroxide (KOH) (9.5 g, 0.17 mol) were introduced at room temperature in a 50 ml round-bottom flask. The reaction mixture was refluxed (60 °C) for 12 hours, cooled down at room temperature and concentrated under vacuum. The residue was introduced in a dialysis membrane with a Molecular Weight Cut-Off (MWCO) of 3.5 kDa and dialyzed in pure MiliQ water in a 2L beaker for 2 days. Finally, the aqueous PAA-*b*-PVP solution was lyophilized to obtain PAA-*b*-PVP as a powder. This final product was characterized by ^{1}H NMR (300 MHz in D_2O) δ ppm (Fig. S3†): range 1.4–1.53 (2nH, –C**H**$_2$–CH(COOH)–), 1.6–1.75 (2mH, –N–CH_2–C**H**$_2$–CH_2–CO(N)), 1.82–2.05 (2mH, –C**H**$_2$–CH($NCH_2CH_2CH_2CO$(N))–), 2.07–2.19 (1nH, –CH_2–C**H**(COOH)–), 2.2–2.5 (2mH, –N–CH_2–CH_2–C**H**$_2$–CO(N)), 3.0–3.35 (2mH, –N–C**H**$_2$–CH_2–CH_2–CO(N)), 3.4–3.8 (1mH, –CH_2–C**H**($NCH_2CH_2CH_2CO$(N))–) and by ATR-FTIR spectroscopy: ν(C═O) PVP ring = 1674 cm^{-1} and ν_{as}(OCO) = 1564 cm^{-1} and ν_{sym}(OCO) = 1402 cm^{-1}.

HPICs preparation

0.5 wt% solution of PAA_{32}-*b*-PVP_{59} were prepared by dissolution of the necessary quantity of the copolymer in Milli-Q water (18.2 mΩ). Gd^{3+}, Eu^{3+} and Y^{3+} stock solutions (65 mM) were prepared by dissolution of $Gd(NO_3)_3{\cdot}6H_2O$, $Eu(NO_3)_3{\cdot}5H_2O$ and $Y(NO_3)_3{\cdot}6H_2O$, respectively in Milli-Q water. HPICs were formed by mixing solutions of PAA_{32}-*b*-PVP_{59} (0.5 wt%) with solutions of Gd^{3+}, Eu^{3+} and Y^{3+}, respectively. Lanthanide ions' concentrations were adjusted in order to vary the molar fraction R = 3·[Ln^{3+}]/[AA] between the positive charges of lanthanide ions and the negative ones of the polymers between 0.2 and 2.2 within the HPICs. After mixing, the pH of the solutions was adjusted to 6.8–7.

Experimental characterization

^{1}H NMR experiments were performed on a 300 MHz Bruker spectrometer using $CDCl_3$ and D_2O as solvent at room temperature. Chemical shifts were reported in ppm.

^{1}H NMR experiments-Y^{3+}-titration were performed on a Bruker Avance 600 MHz spectrometer equipped with a 5 mm triple resonance inverse *Z*-gradient probe (TBI 1H, 31P, BB). The sample were prepared in a mixture of 10% vol. D_2O and 90% vol. H_2O and the pH was adjusted to 7. The temperature was set to 25 °C.

^{1}H spin–lattice relaxation times (T_1) were measured using the excitation sculpting inversion-recovery pulse sequence t1iresgp. The relaxation delay was 6 s and the acquisition time was 1 s. For each measurement, the recovery times were from 50 ms to 6 s and 8 points were collected.

Size exclusion chromatography (SEC) measurements were performed with a system composed of an Agilent technologies guard column (PLGel20 μm, 50 × 7.5 mm) and a set of three columns (TSKgel Alpha-2500, Alpha-3000, Alpha-3500 TOSOH BIOSCIENCE). Detections were realized using a Varian Prostar UV detector (dual wavelength analysis at 290 and 254 nm), a MiniDawn TREOS multi-angle light scattering detector (Wyatt Technology Corporation) and a Wyatt Optilab® rEX refractive index detector. DMF LiBr (10 mM) was used as eluent at 50 °C (flow rate, 1 mL min^{-1}). Prior to injections, the samples were prepared at a concentration of 10 mg mL^{-1} and filtered through a 0.45 μm PTFE filter. Recorded data were treated using the Wyatt Astra 7.1 software. The dn/dc value for the PMA-XA_1 was found to be 0.0558 and for the block copolymer 0.0799 mL g^{-1}. This last one was calculated by using the dn/dc value of the PVP of 0.093 mL g^{-1}.

Mono-angle dynamic light scattering and *zeta potential* measurements were realized using a Zetasizer Nano-ZS (Malvern Instruments, Ltd, UK) with integrated 4 mW He–Ne laser, λ = 633 nm. Light scattering intensity (at 173°) was measured using the same recording parameters for all the samples. In order to obtain *Z*-average sizes of the colloidal structures, the correlation functions were analyzed *via* the cumulant method. For each sample, 5 series of 10 recorded signals of 10 seconds were realized for size data records and only 3 series for zeta potential data, at a controlled temperature of 25 °C.

Multi-angle dynamic light scattering experiments were conducted on a 3D LS spectrometer from LS instruments (Switzerland) at 20 °C. Working with a laser at 660 nm, this instrument recorded light scattering for scattering angles between 15 and 150°. Typical acquisition time for each angle was set to 30 s. All data were then analyzed using a laboratory

made software program (named M-STORMS).[69] Cumulant or NNLS method led to an estimation of the average decay rate Γ for each angle. The linear dependency of Γ *versus* the square of the scattering vector q ($\Gamma = q^2 \cdot D$) gives the diffusion coefficient of the nano-objects and therefore their radius through the Stokes–Einstein equation: $D = \frac{k \cdot T}{6\pi\eta \cdot R_h}$ where T is the temperature and η the viscosity of the solution (taken as the one of pure water).

Transmission electron microscopy (TEM) and high-angle annular dark-field scanning transmission electron microscopy (HAADF-STEM) experiments. Samples were prepared by deposition of one drop of solution containing Gd^{3+}/PAA_{32}-*b*-PVP_{59} HPICs on a carbon coated copper grids (CF200-Cu 200 mesh from Tel Pella Inc.) Low resolution transmission electron microscopy (TEM) measurements were performed on a Hitachi HT7700 device in collaboration with the platform CMEAB from Toulouse. STEM-HAADF analysis were performed on a Field Emission Electron Jeol 2100F Microscope (200 kV), with an electron probe of 1 nm in size, available to Raimond Castaing center of microscopy, Toulouse.

Photophysical experiments. Emission spectra and luminescence decays at room temperature of the Eu HPICs were measured using a Cary Eclipse spectrofluorimeter equipped with a xenon flash lamp source (60–75 kW, flash period 2 to 3 μs) and a Hamamatsu R928 photomultiplier. Time-resolved spectra were recorded with delay step of 100 μs. Lifetimes τ (uncertainty ≤5%) were determined by monitoring the decay at 615 nm, following pulsed excitation. The luminescence decay curves were fitted by an equation of the form $I(t) = I(0)\exp(-t/\tau)$ by using Origin curve-fitting program, where $I(t)$ is the total luminescence intensity at time t, $I(0)$ the luminescence intensity at $t = 0$ ms, and τ is the corresponding lifetime.

ATR-FTIR experiments. All IR measurements were recorded, in a powder form after lyophilization of the HPICs solutions, using a Nicolet 6700 FT-IR spectrometer from Thermo Fischer Scientific in ATR mode on a diamond crystal.

Relaxivity measurements. Longitudinal relaxation times T_1 (ms) were measured at 0.47T using a minispec mq20 relaxometer from Bruker at a constant temperature of 25 °C.

Biological *in vitro* assays

Cell culture. Human HCT-116 colorectal cancer cells (CCL-247) were recently purchased from ATCC and grown in DMEM high 4.5 g l^{-1} glucose, GLUTAMax (Fisher scientific, Waltham, MA, USA) and supplemented with 10% of heat-inactivated fetal bovine serum and 100 U ml^{-1} penicillin, and 100 μg ml^{-1} streptomycin. Cells were maintained at 37 °C in a humidified atmosphere containing 5% CO_2 and used under passage 12. All along the experiments, cells were tested negative for mycoplasma (MycoAlert mycoplasma detection kit, Lonza).

Cytotoxicity experiment. The day before the experiments, 10 000 HCT-116 were seeded in 96-well plates. The day of experiment, cells were incubated for 48 h at 37 °C with increasing concentration of Gd^{3+} and Eu^{3+} HPICs and its individual components, respectively, PAA-*b*-PVP polymer and $Gd(NO_3)_3$ or $Eu(NO_3)_3$ aqueous solutions, at similar concentrations as the ones tested for HPICs. Cell viability was quantified using PrestoBlue reagent (Fisher scientific) according to the manufacturer's instructions. Briefly, after 48 h of incubation, cell culture medium was removed and cells were incubated for 30 min at 37 °C with 100 μl of 1× PrestoBlue reagent diluted in PBS, before reading absorbance on a plate reader at 570 nm and 600 nm Synergy H1 (Biotek, Winooski, VT, USA). Six biological replicates were produced and analyzed for each condition. Data analysis was performed using GraphPad Prism 8 program (GraphPad Software, Inc., La Jolla, CA, USA) and data were expressed as mean ± SEM. Statistical comparisons were performed using one-way analysis of variance (ANOVA) followed by Dunnett's post-test in comparison to the control condition. $*p < 0.05$, $**p < 0.01$, $***p < 0.001$ and $****p < 0.0001$.

Intracellular HPICs quantification by flow cytometry. The day before the experiments, 80 000 HCT-116 were seeded in 12-well plates. Cells were incubated for 6 hours with cell culture medium containing each component of the HPICs, respectively PAA-*b*-PVP polymer alone (0.07 wt%), or $Eu(NO_3)_3$ aqueous solution (0.9 mM) or corresponding Eu-HPICs. An additional set of experiments was performed at 4 °C instead or 37 °C for PAA-*b*-PVP polymer alone (0.07 wt%) condition. After incubation, cells were washed once with PBS and then cells were trypsinized and transferred on ice within a U-bottom 96-well plate. Cells were analyzed with a BD LSR Fortessa flow cytometer equipped with an HTS module for plate reading, using the 405 nm laser for excitation and fluorescence emission was collected using the BV 711A filter, which allowed the detection of the maximum of signal. At least 20 000 events were acquired in each well. Data were analyzed with FlowJo v10 (FlowJo). Three biological replicates were produced and analyzed for each condition. Statistical comparisons were performed using one-way analysis of variance (ANOVA) followed by Tukey's multiple comparison post-test. $*p < 0.05$, $**p < 0.01$, $***p < 0.001$ and $****p < 0.0001$.

Intracellular Eu^{3+} quantification by ICP-MS. Inductively coupled plasma-mass spectrometry (ICP-MS) was used to quantify europium penetration in cells. For that purpose, 20 million of HCT-116 cells grown in 75 cm^2 flask were incubated for 6 h at 37 °C with 0.9 mM $Eu(NO_3)_3$ aqueous solution or the Eu^{3+}/PAA_{32}-*b*-PVP_{59} HPICs. After incubation cells were washed twice with 10 ml of PBS, trypsinized and cell pellets were sent to GLINCS (Villeurbanne, France) for ICP-MS analysis on Nexion 2000 (PerkinElmer).

In vivo experiments

Mice. 6 BALB/cOlaHsd mice (Envigo) aged 10–12 weeks were used for MRI experiments.

All *in vivo* experimental procedures were approved by our institutional animal care and use committee CEEA122 (APAFIS 5192-2016041911336422 and 34703-2022011811542488) and conducted in compliance with the Ethics Committee pursuant to European legislation translated into French Law as Decret 2013-118 dated 1st of February 2013.

Small animal MRI. Animals were anesthetized with isoflurane (induction 3%–4%, maintenance 1.5% (isoflurane/O_2) to insert a catheter in the tail vein. Then, the mice is placed in a specific MRI imaging cell (Minerve, Esternay, France) to preserve the health status (SPF), ensure the temperature regulation and the breathing monitoring. Animals received a dose of 15 μmol kg^{-1} of Gd equivalent (100 μl) (Dotarem®, Guerbet, France) or HPICs followed by a 200 μl flush of saline.

MR image acquisitions were performed on a Biospec 7T dedicated to small animals (Bruker, Wissenbourg, France). Acquisitions of the abdominal images were carried out with a 40 mm transmit-receive volume coil and triggered on breathing to reduce motion artifacts. T_1 weighted images were acquired using Flash sequence with the following parameters: TR = 220 ms; TE = 3.5 ms; flip angle: 40°; number of average: 4; FOV: 40 × 40 mm; resolution 200 × 200 μm; 13 slices of 1 mm thickness; fat suppression; acquisition time: 2 min.

Author contributions

Marjorie Yon: Investigation and writing (supporting); Laure Gibot: investigation, conceptualization (supporting) and writing (supporting); Stéphane Gineste: investigation; Pascale Laborie: investigation; Christian Bijani: investigation; Christophe Mingotaud: validation and methodology and writing (supporting); Olivier Coutelier: validation, supervision (supporting) and writing (supporting); Franck Desmoulin: *in vivo* investigation (lead) and writing (supporting); Carine Pestourie: *in vivo* investigation (supporting); Mathias Destarac: validation and writing (supporting); Diana Ciuculescu-Pradines: conceptualization (equal), methodology (equal), project administration (equal), supervision (equal), writing (equal); Jean-Daniel Marty: conceptualization (equal), methodology (equal), project administration (equal), supervision (equal), writing (equal).

Data availability statement

The data that support the findings of this study are available from the corresponding author upon reasonable request.

Conflicts of interest

There are no conflicts to declare.

Acknowledgements

The authors acknowledge the Imaging Core Facility TRI-IPBS, (Toulouse) and more precisely Penelope Viana for her help with the flow cytometry experiments, the CMEAB platform, (Toulouse) for TEM facilities, Laurent Weingarten for the HAADF-STEM analysis and the Raimond Castaing microcharacterization platform facilities, (Toulouse), Technopolym service and ICT (Institut de Chimie de Toulouse) (ICT-UAR 2599) **https://www.ict.ups-tlse.fr** for the Size Exclusion Chromatography analysis, 300 MHz NMR and IR facilities, LSPCMIB laboratory (Toulouse) for the access to the luminescent spectroscopy facilities, LCC laboratory (Toulouse) for the 600 MHz NMR facilities, Chantal Galaup and Marc Guerre for the fruitful discussions, the doctoral school Science de la Matiere de Toulouse, the Ministère de l'Enseignement Supérieur et de la Recherche and Toulouse Tech Transfer for the financial support.

References

1 S. S. Syamchand and G. Sony, *J. Lumin.*, 2015, **165**, 190–215.
2 J. Wahsner, E. M. Gale, A. Rodríguez-Rodríguez and P. Caravan, *Chem. Rev.*, 2019, **119**, 957–1057.
3 A. El Jundi, S. J. Buwalda, Y. Bakkour, X. Garric and B. Nottelet, *Adv. Colloid Interface Sci.*, 2020, **283**, 102213.
4 A. Harada and K. Kataoka, *Polym. J.*, 2018, **50**, 95–100.
5 B. V. K. J. Schmidt, *Macromol. Chem. Phys.*, 2018, **219**, 1700494.
6 D. Taton, A.-Z. Wilczewska and M. Destarac, *Macromol. Rapid Commun.*, 2001, **22**, 1497–1503.
7 C. Frangville, Y. Li, C. Billotey, D. R. Talham, J. Taleb, P. Roux, J.-D. Marty and C. Mingotaud, *Nano Lett.*, 2016, **16**, 4069–4073.
8 M. Yon, S. Gineste, G. Parigi, B. Lonetti, L. Gibot, D. R. Talham, J.-D. Marty and C. Mingotaud, *ACS Appl. Nano Mater.*, 2021, **4**, 4974–4982.
9 N. M. Pinkerton, L. Behar, K. Hadri, B. Amouroux, C. Mingotaud, D. R. Talham, S. Chassaing and J.-D. Marty, *Nanoscale*, 2017, **9**, 1403–1408.
10 H.-W. Shin, H. Sohn, Y.-H. Jeong and S.-M. Lee, *Langmuir*, 2019, **35**, 6421–6428.
11 Y.-H. Jeong, H.-W. Shin, J.-Y. Kwon and S.-M. Lee, *ACS Appl. Mater. Interfaces*, 2018, **10**, 23617–23629.
12 E. Seo, J. Kim, Y. Hong, Y. S. Kim, D. Lee and B.-S. Kim, *J. Phys. Chem. C*, 2013, **117**, 11686–11693.
13 H. J. Lee, S. E. Kim, I. K. Kwon, C. Park, C. Kim, J. Yang and S. C. Lee, *Chem. Commun.*, 2010, **46**, 377–379.
14 S. Tanaka, J. Lin, Y. V. Kaneti, S. Yusa, Y. Jikihara, T. Nakayama, M. B. Zakaria, A. A. Alshehri, J. You, Md. S. A. Hossain and Y. Yamauchi, *Nanoscale*, 2018, **10**, 4779–4785.
15 S. Gineste, B. Lonetti, M. Yon, J. Giermanska, E. Di Cola, M. Sztucki, Y. Coppel, A. F. Mingotaud, J. P. Chapel, J. D. Marty and C. Mingotaud, *J. Colloid Interface Sci.*, 2022, **9**, 698.
16 X. Zhang, K. Wang, M. Liu, X. Zhang, L. Tao, Y. Chen and Y. Wei, *Nanoscale*, 2015, **7**, 11486–11508.
17 K. Zhang, M. C.-L. Yeung, S. Y.-L. Leung and V. W.-W. Yam, *Chem*, 2017, **2**, 825–839.
18 G. Pound, F. Aguesse, J. B. McLeary, R. F. M. Lange and B. Klumperman, *Macromolecules*, 2007, **40**, 8861–8871.

19 K. H. Markiewicz, L. Seiler, I. Misztalewska, K. Winkler, S. Harrisson, A. Z. Wilczewska, M. Destarac and J.-D. Marty, *Polym. Chem.*, 2016, **7**, 6391–6399.
20 M. Mohamed, A. S. Abu Lila, T. Shimizu, E. Alaaeldin, A. Hussein, H. A. Sarhan, J. Szbeni and T. Ishida, *Sci. Technol. Adv. Mater.*, 2019, **20**, 710.
21 K. Knop, R. Hoogenboom, D. Fischer and U. S. Schubert, *Angew. Chem., Int. Ed.*, 2010, **49**, 6288.
22 M. C. Castells and E. J. Phillips, *N. Engl. J. Med.*, 2021, **384**(7), 643.
23 L. Luo, M. Ranger, D. G. Lessard, D. Le Garrec, S. Gori, J.-C. Leroux, S. Rimmer and D. Smith, *Macromolecules*, 2004, **37**, 4008–4013.
24 Y. Luo, Y. Hong, L. Shen, F. Wu and X. Lin, *AAPS PharmSciTech*, 2021, **22**, 34.
25 A. Benahmed, M. Ranger and J. Leroux, *Pharm. Res.*, 2001, **18**, 323–328.
26 T. Song, F. Gao, S. Guo, Y. Zhang, S. Li, H. You and Y. Du, *Nanoscale*, 2021, **13**, 3895–3910.
27 H. A. Ravin, A. M. Seligman and J. Fine, *N. Engl. J. Med.*, 1952, **247**, 921–929.
28 J. A. Brydson, *Plast. Mater*, Elsevier, 1999, pp. 466–477.
29 V. P. Torchilin, *J. Microencapsulation*, 1998, **15**, 1.
30 S. Aroua, E. G. V. Tiu, M. Ayer, T. Ishikawa and Y. Yamakoshi, *Polym. Chem.*, 2015, **6**, 2616–2619.
31 M. A. de Farias and M. do C. Gonçalves, *Polímeros*, 2016, **26**, 1–10.
32 T. M. Amis, J. Renukuntla, P. K. Bolla and B. A. Clark, *Pharmaceutics*, 2020, **12**, 892.
33 M.-K. Chun, C.-S. Cho and H.-K. Choi, *J. Appl. Polym. Sci.*, 2004, **94**, 2390–2394.
34 M.-K. Chun, C.-S. Cho and H.-K. Choi, *J. Controlled Release*, 2002, **81**, 327–334.
35 Z. S. Nurkeeva, V. V. Khutoryanskiy, G. A. Mun, A. B. Bitekenova, S. Kadlubowski, Y. A. Shilina, P. Ulanski and J. M. Rosiak, *Colloids Surf., A*, 2004, **236**, 141–146.
36 T. Swift, C. C. Seaton and S. Rimmer, *Soft Matter*, 2017, **13**, 8736–8744.
37 R. Liang, S. You, L. Ma, C. Li, R. Tian, M. Wei, D. Yan, M. Yin, W. Yang, D. G. Evans and X. Duan, *Chem. Sci.*, 2015, **6**, 5511–5518.
38 A. Guinaudeau, O. Coutelier, A. Sandeau, S. Mazières, H. D. Nguyen Thi, V. Le Drogo, D. J. Wilson and M. Destarac, *Macromolecules*, 2014, **47**, 41–50.
39 M. Jacquin, P. Muller, G. Lizarraga, C. Bauer, H. Cottet and O. Théodoly, *Macromolecules*, 2007, **40**, 2672–2682.
40 M. Mestivier, J. R. Li, A. Camy, C. Frangville, C. Mingotaud, F. Benoît-Marquié and J. Marty, *Chem. – Eur. J.*, 2020, **26**, 14152–14158.
41 J. Loos, E. Sourty, K. Lu, G. de With and S. v. Bavel, *Macromolecules*, 2009, **42**, 2581–2586.
42 S. Mourdikoudis, R. M. Pallares and N. T. K. Thanh, *Nanoscale*, 2018, **10**, 12871–12934.
43 K. Binnemans, *Coord. Chem. Rev.*, 2015, **295**, 1–45.
44 R. M. Supkowski and W. DeW. Horrocks, *Inorg. Chim. Acta*, 2002, **340**, 44–48.
45 S. A. Cotton and P. R. Raithby, *Coord. Chem. Rev.*, 2017, **340**, 220–231.
46 J. Zhang, Y. Liu, Y. Li, H. Zhao and X. Wan, *Angew. Chem.*, 2012, **124**, 4676–4680.
47 G. Deacon, *Coord. Chem. Rev.*, 1980, **33**, 227–250.
48 C. C. R. Sutton, G. da Silva and G. V. Franks, *Chem. – Eur. J.*, 2015, **21**, 6801–6805.
49 H. G. Brittain, F. S. Richardson and R. B. Martin, *J. Am. Chem. Soc.*, 1976, **98**, 8255–8260.
50 S. A. Cotton, in *EIBC*, ed. R. A. Scott, John Wiley & Sons, Ltd, Chichester, UK, 2011, p. eibc0195.
51 S. Majeed and S. A. Shivashankar, *J. Mater. Chem. C*, 2014, **2**, 2965.
52 F. Chen, X. H. Zhang, X. D. Hu, W. Zhang, R. Zeng, P. D. Liu and H. Q. Zhang, *J. Alloys Compd.*, 2016, **664**, 311–316.
53 J.-G. Kang, B.-K. Min and Y. Sohn, *Ceram. Int.*, 2015, **41**, 1243–1248.
54 Y. Jia, T. Luo, X.-Y. Yu, B. Sun, J.-H. Liu and X.-J. Huang, *RSC Adv.*, 2013, **3**, 15805.
55 J. Zhang, L. Dai, A. M. Webster, W. T. K. Chan, L. E. Mackenzie, R. Pal, S. L. Cobb and G. Law, *Angew. Chem., Int. Ed.*, 2021, **60**, 1004–1010.
56 J. Yu, D. Parker, R. Pal, R. A. Poole and M. J. Cann, *J. Am. Chem. Soc.*, 2006, **128**, 2294–2299.
57 S. Sachs, A. Heller, S. Weiss, F. Bok and G. Bernhard, *Toxicol. In Vitro*, 2015, **29**(7), 1555.
58 M. Sy, A. Nonat, N. Hildebrandt and L. J. Charbonnière, *Chem. Commun.*, 2016, **52**, 5080–5095.
59 D. Parker and J. Yu, *Chem. Commun.*, 2005, 3141.
60 C. De Rosa, A. Melchior, M. Sanadar, M. Tolazzi, A. Giorgetti, R. P. Ribeiro, C. Nardon and F. Piccinelli, *Inorg. Chem.*, 2020, **59**, 12564–12577.
61 M. A. Condrau, R. A. Schwendener, P. Niederer and M. Anliker, *Cytometry*, 1994, **16**, 187–194.
62 G. Song, Y. Lin, Z. Zhu, H. Zheng, J. Qiao, C. He and H. Wang, *Macromol. Rapid Commun.*, 2015, **36**, 278–285.
63 M. Rohrer, H. Bauer, J. Mintorovitch, M. Requardt and H.-J. Weinmann, *Invest. Radiol.*, 2005, **40**, 715.
64 G. Zhang, R. Zhang, X. Wen, L. Li and C. Li, *Biomacromolecules*, 2008, **9**, 36–42.
65 P. Mi, H. Cabral, D. Kokuryo, M. Rafi, Y. Terada, I. Aoki, T. Saga, I. Takehiko, N. Nishiyama and K. Kataoka, *Biomaterials*, 2013, **34**, 492–500.
66 Z. Mo, Q. Li, K. Zhao, Q. Xu, H. Hu, X. Chen, Y. Luo, B. Chi, L. Liu, X. Fang, G. Liao, Z. Xu, J. Wang and S. Yang, *ACS Appl. Mater. Interfaces*, 2022, **14**(8), 10001–10014.
67 Z. Mo, M. Qiu, K. Zhao, H. Hu, Q. Xu, J. Cao, Y. Luo, L. Liu, Z. Xu, C. Yi, Z. Xiong, G. Liao and S. Yang, *J. Colloid Interface Sci.*, 2022, **611**, 193–204.
68 X. Liu, O. Coutelier, S. Harrison, T. Tassaing, J.-D. Marty and M. Destarac, *ACS Macro Lett.*, 2015, **4**, 89.
69 M. Dionzou, A. Morère, C. Roux, B. Lonetti, J. D. Marty, C. Mingotaud, P. Joseph, D. Goudounèche, B. Payré, M. Léonetti and A. F. Mingotaud, *Soft Mater.*, 2016, **12**, 2166–2176.